Electronic Supplementary Material (ESI) for Chemical Communications.

Supporting Information

Ultrafine PtCoRh Nanorods for Efficient Hydrogen Evolution Reaction in Acid

Content

Experimental section.

Chemicals. Platinum(II) acetylacetonate ($Pt(acac)_2$, 97%), cobalt(III) acetylacetonate ($Co(acac)_3$, ≥99.99%), didodecyldimethylammonium bromide (DDAB, 98.0%), polyvinylpyrrolidone (PVP, average mol. wt. 40,000), hexadecyl trimethyl ammonium bromide (CTAB, ~99%), and sodium dodecyl sulfate (SDS, ≥98.5%) were purchased from Sigma-Aldrich. Rhodium(III) acetylacetonate ($Rh(acac)_3$, 97%) was obtained from J&K Scientific Ltd. Molybdenum hexacarbonyl ($Mo(CO)_6$, 98%) was received from Sinopharm Chemical Reagent Co. Ltd. Oleylamine (OAm, 80-90%) was obtained from Aladdin Industrial Co. Cyclohexane (AR) was ordered from Tianjin Kemiou Chemical Reagent Co. Ltd. Commercial Pt/C (20 wt%) was received from Johnson Matthey Chemical Co. Ltd. and commercial IrO_2 was purchased from Macklin Biochemical Co. Ltd. Nafion 212 membrane (~50 μm) and Nafion resin solution (5 wt%) were obtained from DuPont. Gas diffusion layer (GDL, ~0.4875 mm) was obtained from Sunrise Power Co. Ltd. All of the above chemicals were used as received without further purification. Carbon black (Ketjenblack EC600 JD) was obtained from Akzo Nobel and was pretreated in nitric acid (3 M) at 80 °C for 1 h before use. The ultrapure water (18.2 MΩ cm at 25 °C) was produced from a Millipore water system (Synergy® UV) and used in all experiments.

Synthesis of PtCoRh NRs. In a typical synthesis, $Pt(acac)_2$ (10 mg, 0.025 mmol), $Co(acac)_3$ (9 mg, 0.025 mmol)[1-3], $Rh(acac)_3$ (1 mg, 0.0025 mmol) and DDAB (90 mg, 0.194 mmol) were mixed with 5 mL of OAm in a glass tube under 1 hour of mild sonication at ambient conditions. $Mo(CO)_6$ (30 mg, 0.114 mmol) was then added, followed by 5 min of N_2 purging. Next, the reation vessel was heated to 185 °C in an oil bath and incubated at this temperature for 5 h. After being cooled down to room temperature naturally, PtCoRh NRs were purified by centrifuge at 8,000 rpm for 5 min with mixed ethanol and cyclohexane for three times. Eventually, PtCoRh NRs were dispersed in 4 mL of cyclohexane for use. For comparison, PtCo NRs and PtCoRh NRs at different Pt/Co/Rh molar ratios were also synthesized with 0, 2, and 3 mg of $Rh(acac)_3$, respectively, while holding the other synthetic parameters constant.

Synthesis of PtCoRh/C and PtCo/C. 8 mg carbon black (EC600) and 4 mL ethanol were mixed with certain amount of PtCoRh NRs or PtCo NRs suspended in cyclohexane. After 1 hour of mild sonication, carbon supported PtCoRh NRs (PtCoRh/C) and PtCo NRs (PtCo/C) were collected by centrifuge at 4000 rpm, then dried at 70 °C for 2 h in an oven.

Characterizations.

TEM was carried out on a Tecnai G2 F30 Spirit (FEI) operated at 120 kV. HR-STEM, HAADF-STEM, and EDS elemental mapping as well as linear scan profiles were recorded on a JEM-ARM200F (JEOL, 200 keV). A SmartLab 9 kW (Rigaku) at 45 kV and 200 mA was used to collect XRD with Cu Kα radiation (λ = 1.5406 Å) in a 2θ range from 10 to 90°. XPS was collected on a ESCALAB XI+ (Thermo Scientific) with monochromatized Al Kα (1486.6 eV) as the photon source. The neutralizer was used for the XPS

measurements. The raw data of C 1s were deconvoluted as shown in Fig. S25, and the surface sp^2 C (C-H bond) at 284.8 ± 0.1 eV was used to carry out the calibration.[4-6] ICP-OES (Optima 2000DV PerkinElmer) was used to analyze the compositions of samples. TGA curves were recorded on a TA-Q600 in a temperature range from room temperature to 800 °C at a heating rate of 10 °C min^{-1} in dry air. XANES (Rh K-edge) was collected at BL14W1 beamline of Shanghai Synchrotron Radiation Facility (SSRF). The storage ring of SSRF was operated at 3.5 GeV with a stable current of 200 mA. Data collection was carried out in fluorescence mode using Lytle detector and Si(311) double-crystal monochromator under ambient conditions. Pd foil was used as reference to calibrate energy.

Electrochemical measurements.

A CHI760D electrochemical workstation (Shanghai Chenhua Instruments Ltd.) was used to evaluate electrocatalysts with a glassy carbon rotating disk electrode (RDE, 5 mm in diameter) as the working electrode (WE), a carbon rod as the counter electrode, and a Hg/Hg_2SO_4 (saturated K_2SO_4) as the reference electrode (RE)[7, 8]. Besides, certain amount of electrocatalyst was dispersed in the mixture of ultrapure water/ethanol/Nafion (5 wt%) at a volume ratio of 1:9:0.06, followed by 5 min of mild sonication in a water bath cleaner to obtain 1 mg mL^{-1} of electrocatalyst ink. RDE was polished with 5 μm and 30-50 nm alumina paste, and then cleaned with ethanol and ultrapure water. 10 μL of the ink was dropped onto the surface of the polished RDE to reach a metal loading of about 10 $\mu g_{metal}\ cm_{disk}^{-2}$. All the RDE tests were performed in N_2-saturated 0.5 M H_2SO_4 aqueous solution at 25 °C. Cyclic voltammetry (CV) tests between 0-1.2 V (vs. RHE) with a scanning rate of 100 mV s^{-1} was performed to clean the electrocatalysts surface. HER polarization curves were recorded by linear sweep voltammetry (LSV) with a negative sweep rate of 5 mV s^{-1} and a rotation rate of 1600 rpm. Stability test was carried out by potential cycling from -0.1 to 0.3 V (vs. RHE) at a scanning rate of 100 mV s^{-1}. LSV curves were recorded at every 250 cycles to monitor the change of HER activity. Internal resistance (iR) was obtained by using 'iR compensation' function of CHI760D, followed by manual compensation of raw data.

ECSA was assessed by CO stripping in 0.5 M H_2SO_4 aqueous solution at 25 °C. Firstly, high purity N_2 (99.999%) was bubbled through the electrolyte for 20 min to remove air. Next, CO (99.9%) was bubbled for 10 min to saturate the electrolyte with the WE held at 0.1 V (vs. RHE). In the following, N_2 was purged again for another 10 min to remove non-adsorbed CO. Lastly, CO stripping was recorded by collecting CV between 0-1.2 V (vs. RHE) with a scanning rate of 20 mV s^{-1}. The equation (1) for calculating ECSA is as follows:

$$\mathrm{ECSA} = \frac{\mathrm{Q_{CO}}}{420\ \mu\mathrm{C\ cm^{-2}} \cdot \mathrm{m_{Pt}}} \tag{1}$$

Q_{CO} is the CO oxidation charge by integrating CV curve from 0.33 to 1.20 (vs. RHE). 420 μC cm^{-2} is the coulombic charge required for the oxidation of a monolayer of CO. $\mathrm{m_{Pt}}$ is the mass of Pt on RDE.

TOF was calculated according to the following equation (2):

$$\mathrm{TOF} = \frac{\text{Number of hydrogen molecules (per current density)} \times \text{current density}}{\text{Density of active sites}} \tag{2}$$

The number of hydrogen molecules generated per unit time per active site was calculated according to equation (3):

Number of hydrogen molecules

$$= \left(1\ \frac{\mathrm{mA}}{\mathrm{cm}^2}\right)\left(\frac{1\ \mathrm{C\ s^{-1}}}{1000\ \mathrm{mA}}\right)\left(\frac{1\ \mathrm{mol\ e}}{96485.3\ \mathrm{C}}\right)\left(\frac{1\ \mathrm{mol\ H_2}}{2\ \mathrm{mol\ e}}\right)\left(\frac{6.02\times10^{23}\ \mathrm{molecules\ H_2}}{1\ \mathrm{mol\ H_2}}\right) \quad (3)$$

$$= 3.12\times10^{15}\ \mathrm{H_2\ s^{-1}\ cm^{-2}\ per}\ \frac{\mathrm{mA}}{\mathrm{cm}^2}$$

PEMWE single cell testing.

2 mg mL^{-1} of cathode and anode ink was prepared by dispersing PtCoRh/C and commercial IrO_2 (Macklin Biochemical Co. Ltd) in the mixture of ultrapure water, Nafion and ethanol, followed by being sprayed to each side of a membrane (Nafion 212). The mass proportion of Nafion in the catalyst layer is 23 wt%. The cathode and anode consist of 0.1 mg_{Pt} cm^{-2} and 2 mg_{Ir} cm^{-2}, respectively. Then the membrane electrode was sandwiched in-between two pieces of gas diffusion layer (GDL, SUNRISE POWER Co., Ltd) under a pressure of 0.15 MPa for 2 min at 130 °C to form a membrane electrode assembly (MEA).

After assembling MEA in a 4 cm^2 single cell with a torque of 5 N m, ultrapure water was pumped to the anode side at 20 mL min^{-1}. Polarization curves were recorded on a PSW 30-36 direct-current power supply (Good Will Instrument Co., Ltd.) by increasing the current density from 0 to 2 A cm^{-2} at 80 °C and atmospheric pressure. Stability test was operated at 0.1 A cm^{-2} for at least 166 min. Electrochemical impedance spectroscopy (EIS) was carried out at 1.45 V by applying an AC amplitude of 10 mV over the AC frequency range from 10 kHz to 100 Hz on an Autolab potentiostat/galvanostat (Echo Chemie BV Model PGSTAT-302N).

Computational method.

DFT calculations were performed by using Vienna Ab-initio Simulation Package[9, 10] (VASP) under Projected Augmented Wave[11] (PAW) method. Perdew-Burke-Ernzerhof (RPBE) functional was used to describe the exchange and correlation effects with a cutoff energy set at 500 eV[12-14]. (111) plane was chosen to represent electrocatalytic surface. Slab models were constructed with five atomic layers, where the bottom three layers were kept fixed and the top two layers were allowed to relax during structural optimization. Monkhorst-Pack grids[15] were set to be 3×3×1 and 3×3×1 for structural optimizations and density of states (DOS) calculations, respectively. At least 20 Å vacuum layer was applied in z-direction of the slab models, preventing the slabs from vertical interactions.

The free energy of hydrogen adsorption (ΔG_{H^*}) was employed as the activity descriptor toward acidic HER,[16] which is a two-step process and involves only one reaction intermediate, the chemisorbed H atom. The free energy of the adsorbed hydrogen is defined as equation (4):

$$\Delta G_{H^*} = \Delta E_H + \Delta E_{ZPE} - T\Delta S_H \quad (4)$$

where ΔE_H is the hydrogen binding energy, ΔE_{ZPE} is the zero point energy difference between adsorbed

hydrogen and gaseous hydrogen, and TΔS is the corresponding entropy difference between these two states. According to previous studies[16], we used a 0.24 eV value to represent the correction of zero point energy and entropy of hydrogen state.

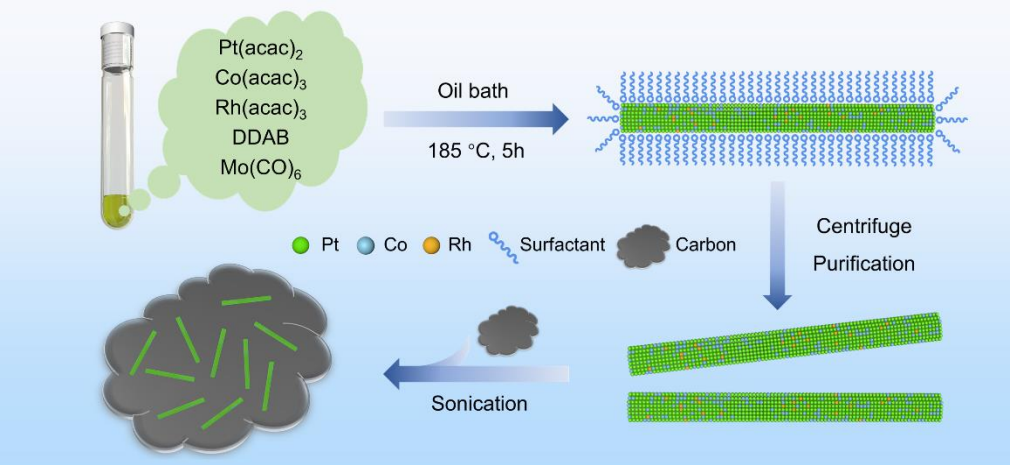

Figure S1 Schematic diagram of the synthetic process of PtCoRh/C NRs.

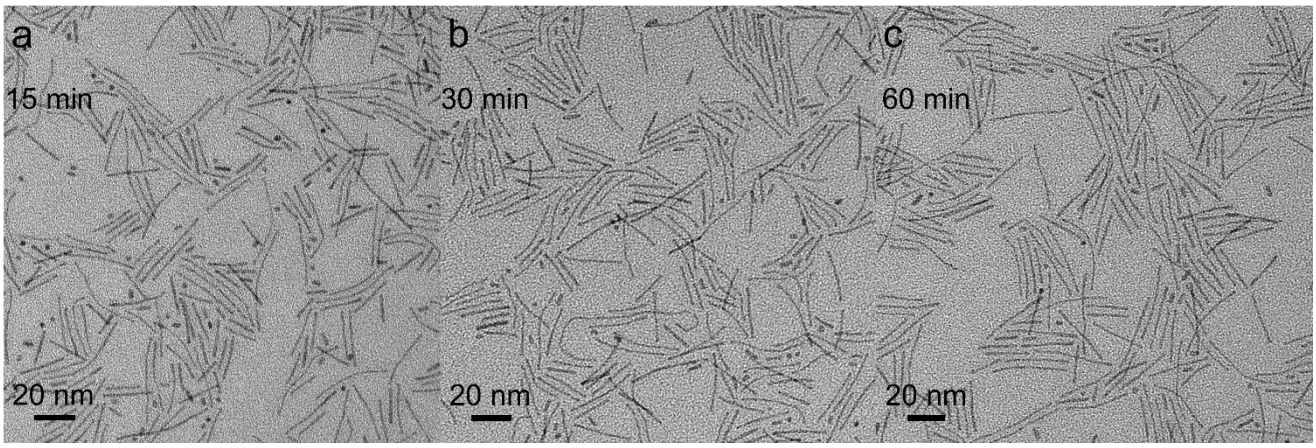

Figure S2 TEM images of the products collected at different reaction time: (a) 15 min; (b) 30 min; (c) 60 min. The number of individual nanoparticles decreases gradually with the reaction time. This suggests that metal salt precursors might nucleate at the beginning and then grow into NRs via oriented attachment and Ostwald ripening[3, 17, 18].

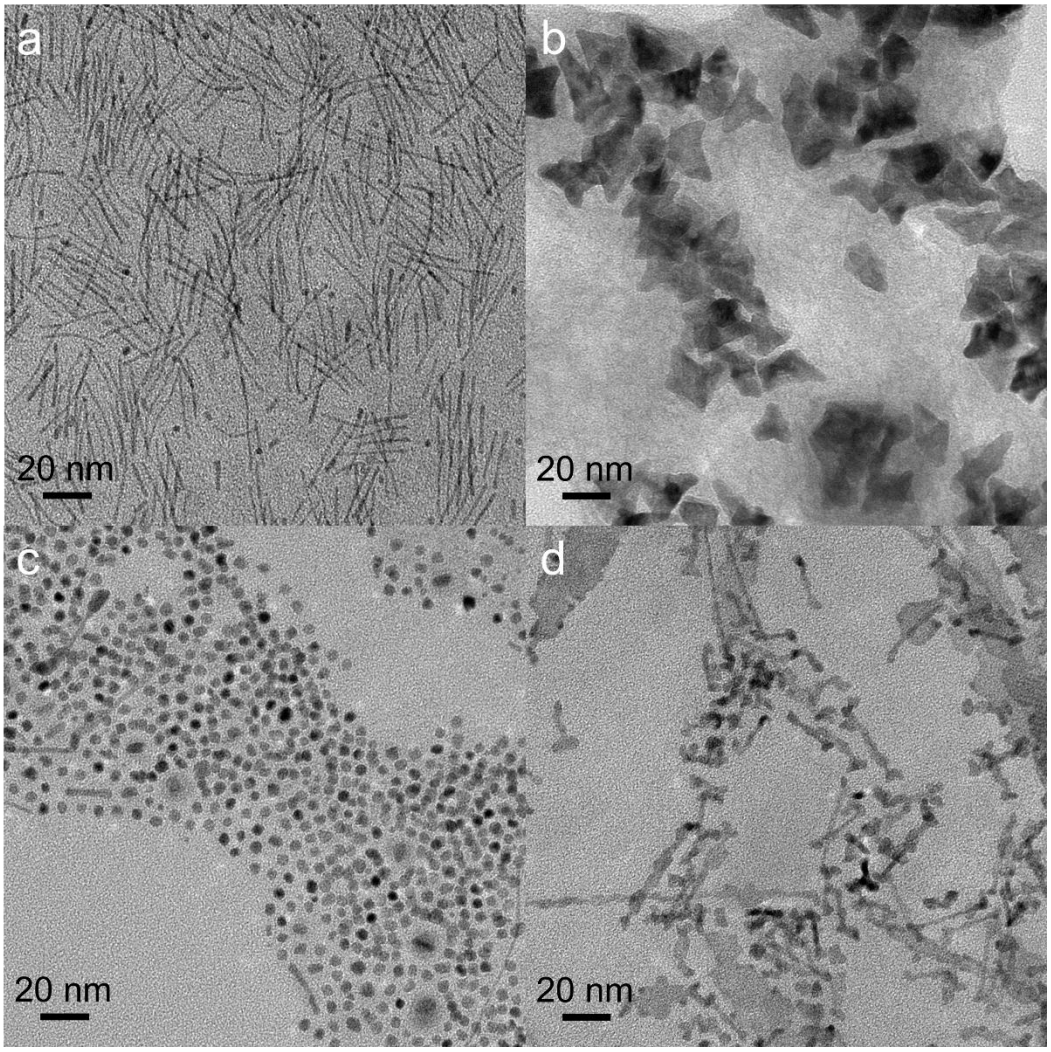

Figure S3. TEM images of the products obtained by varying only one parameter while holding all the other the same as those of ultrafine PtCoRh NRs: (a) in the absence of N_2 purging; (b) in the absence of $Mo(CO)_6$; DDAB was replaced by PVP (c) or SDS (d). Thus, if we omitted N_2, removed $Mo(CO)_6$ or replaced DDAB with other surfactants in the synthesis, the NRs cannot be obtained.

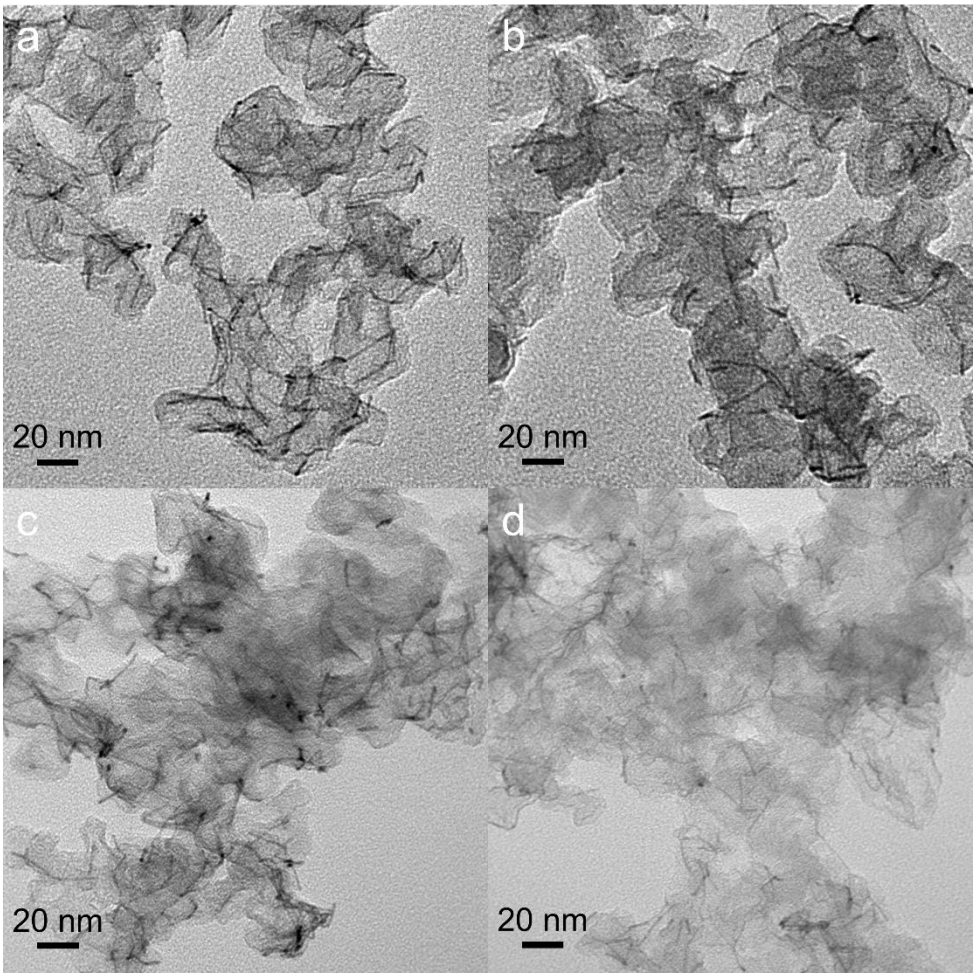

Figure S4. TEM images of (a) PtCoRh/C synthesized with 1 mg of $Rh(acac)_3$; (b) PtCoRh/C-2 synthesized with 2 mg of $Rh(acac)_3$; (c) PtCoRh/C-3 synthesized with 3 mg of $Rh(acac)_3$; (d) PtCo/C synthesized without $Rh(acac)_3$.

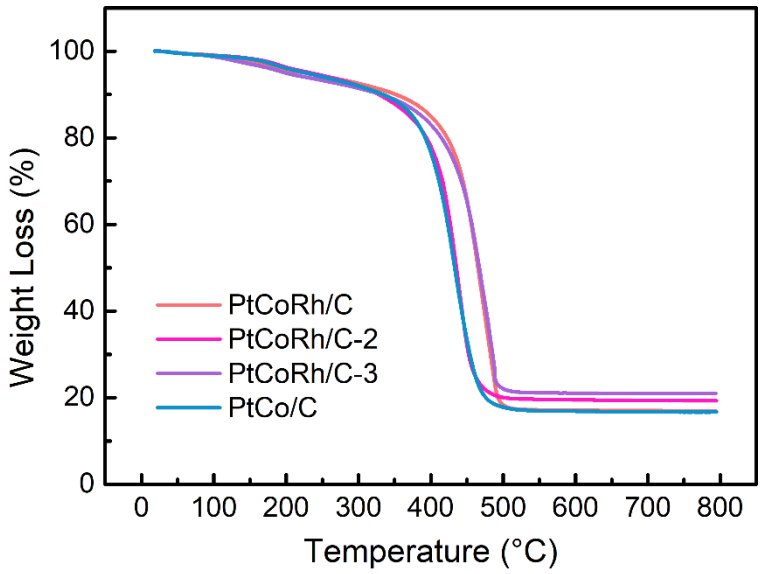

Figure S5. TGA curves of PtCoRh/C, PtCoRh/C-2, PtCoRh/C-3, and PtCo/C.

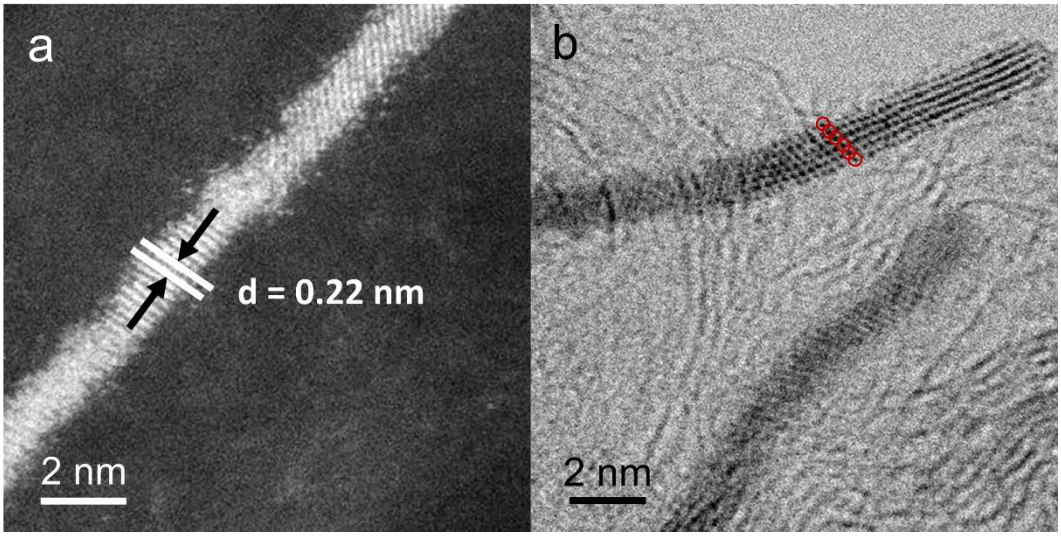

Figure S6. (a) HAADF-STEM and (b) HR-STEM images of PtCoRh/C. Red rings in Fig. b show the NR is only 6 atomic layers in thickness.

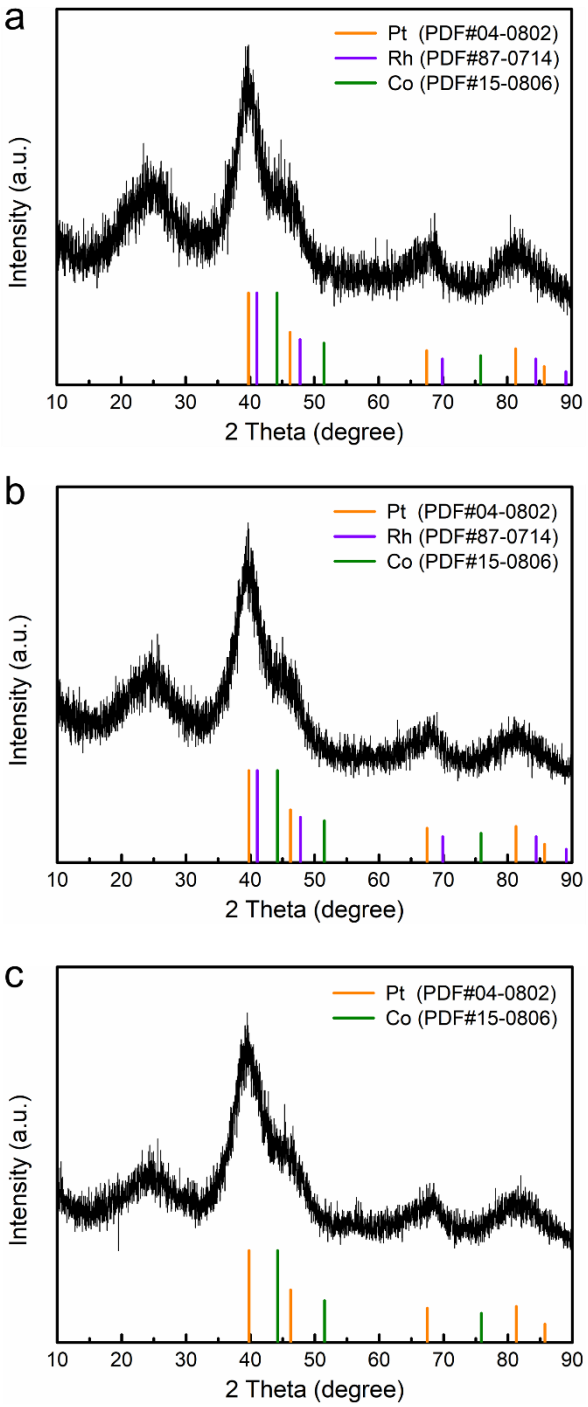

Figure S7. XRD patterns of (a) PtCoRh/C-2, (b) PtCoRh/C-3 and (c) PtCo/C. This series of PtCoRh/C and PtCo/C all exhibit fcc structure.

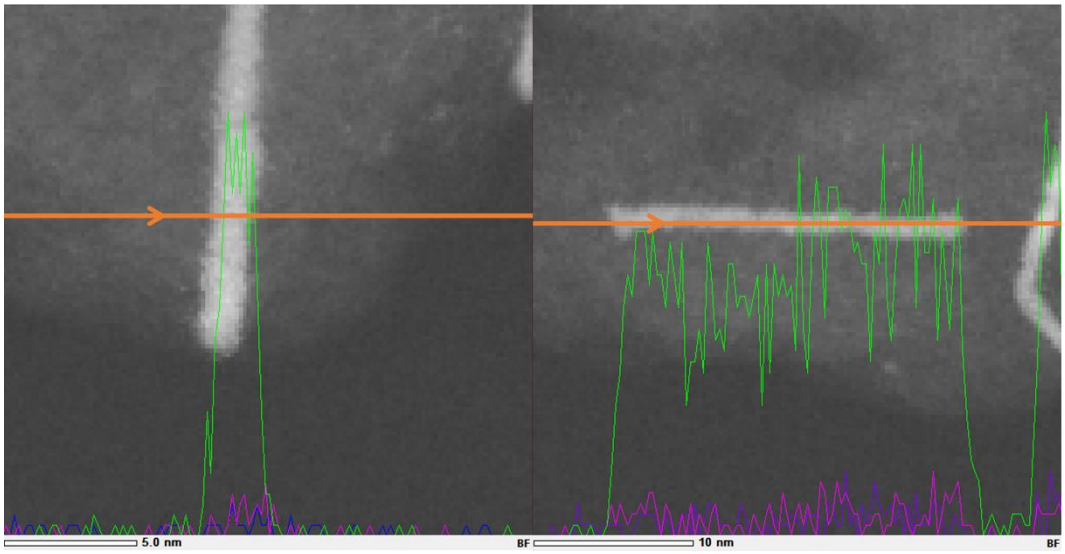

Figure S8. EDS line-scanning profiles of PtCoRh/C. Green for Pt, blue for Co, and pink for Rh.

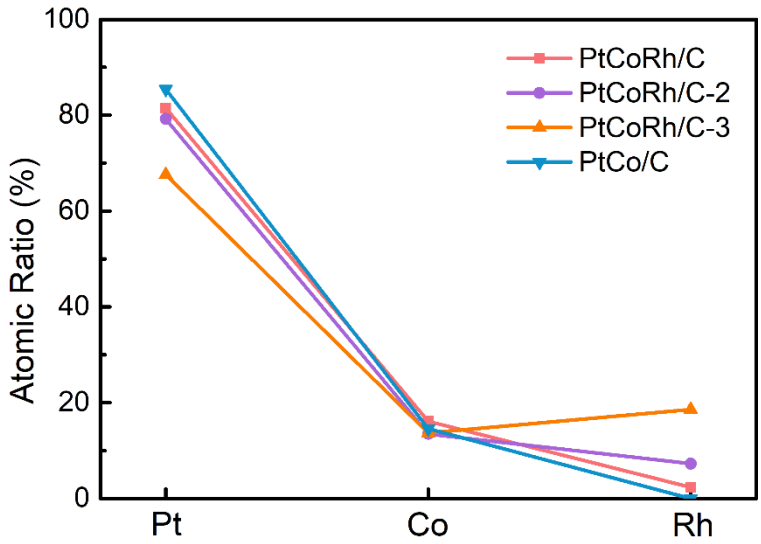

Figure S9. Metallic compositions of PtCoRh/C, PtCoRh/C-2, PtCoRh/C-3, and PtCo/C.

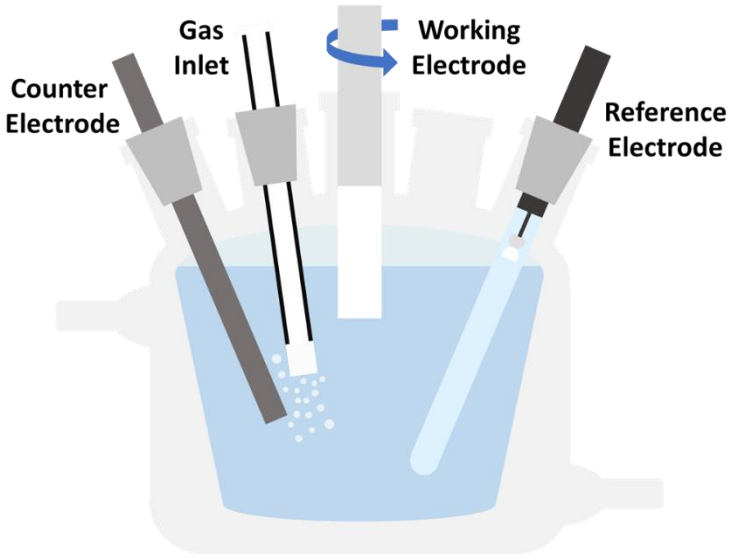

Figure S10. Diagram of three-electrode system for electrochemical tests.

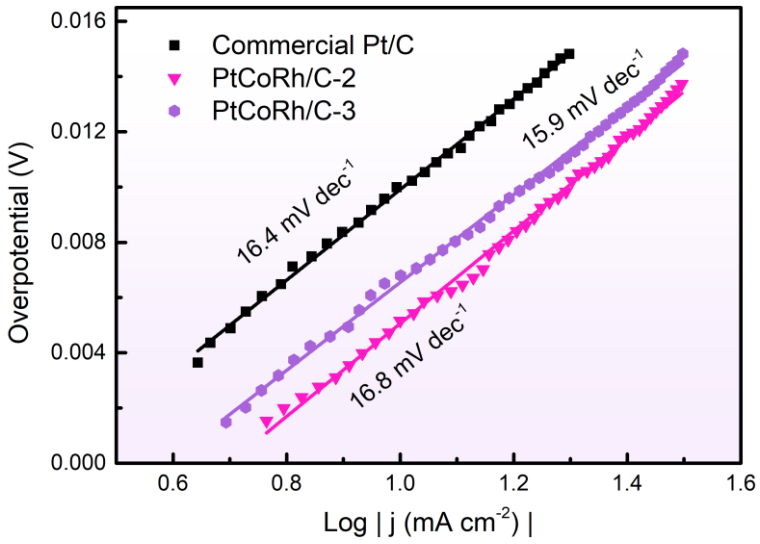

Figure S11. Tafel plots of PtCoRh/C-2, PtCoRh/C-3 and commercial Pt/C.

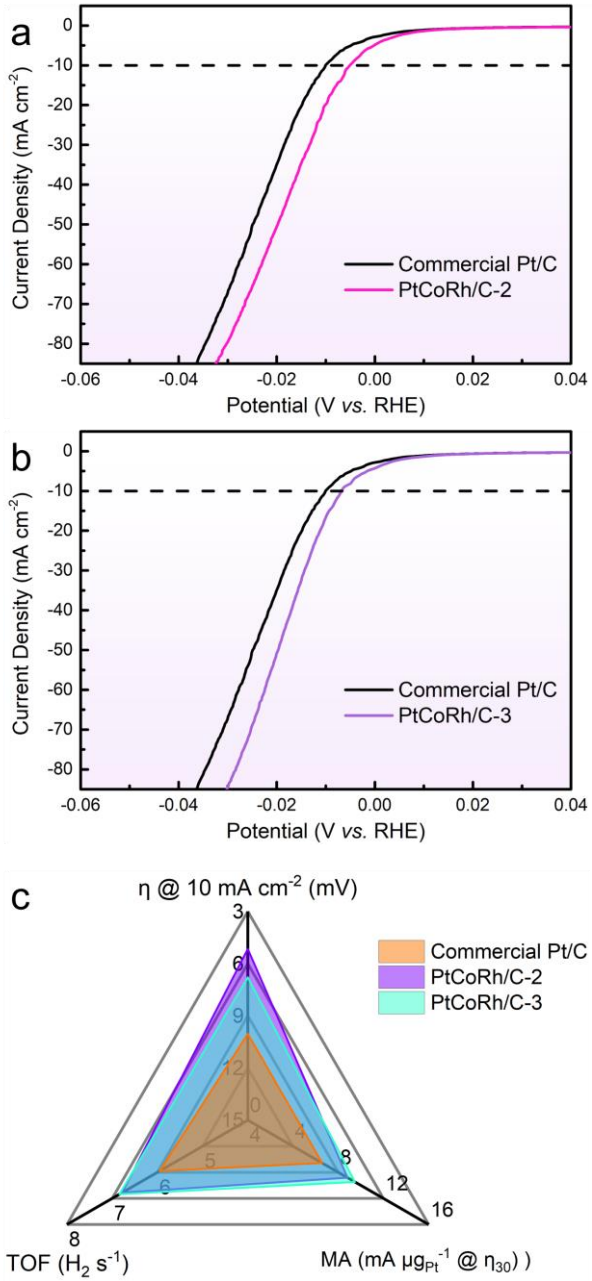

Figure S12. (a, b) IR compensated HER polarization curves of PtCoRh/C-2, PtCoRh/C-3 and commercial Pt/C recorded in N_2-saturated 0.5 M H_2SO_4 aqueous solution; (c) Radar graph of the overpotential, TOF, and MA value derived from the polarization curves. PtCoRh/C-2 and PtCoRh/C-3 show better performances than those of commercial Pt/C, but the MA and TOF values are lower than those of PtCoRh/C.

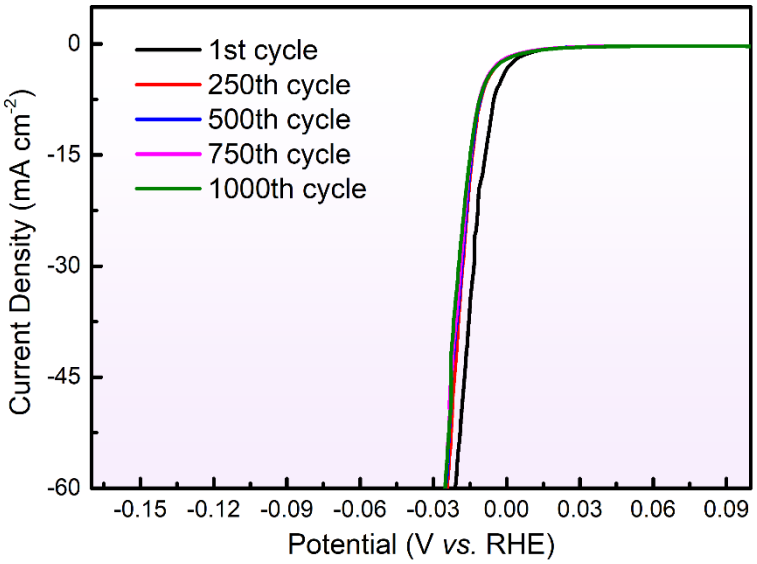

Figure S13. IR compensated polarization curves of PtCoRh/C at every 250 cycles.

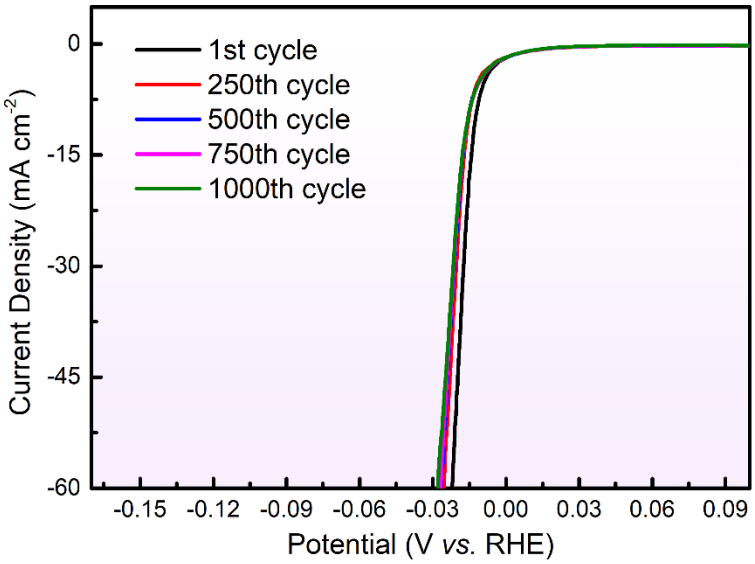

Figure S14. IR compensated polarization curves of commercial Pt/C at every 250 cycles.

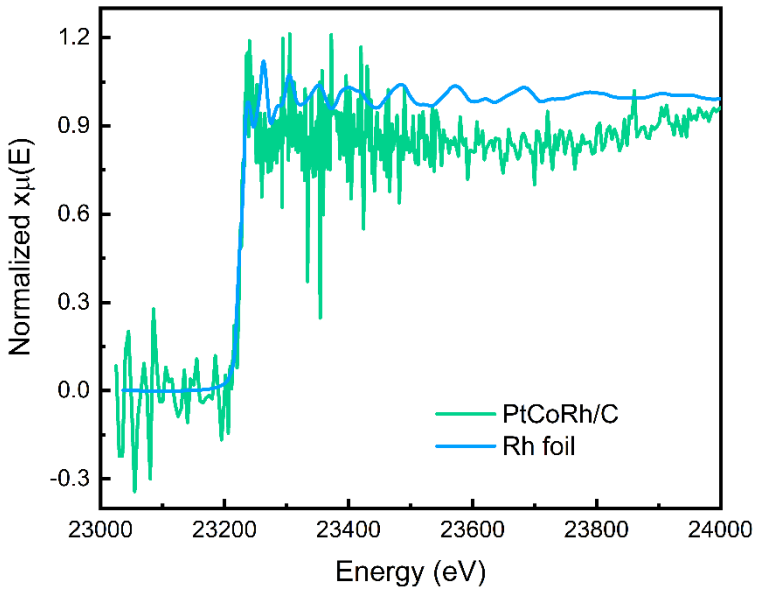

Figure S15. XANES of PtCoRh/C at Rh K-edge with Rh foil for comparison.

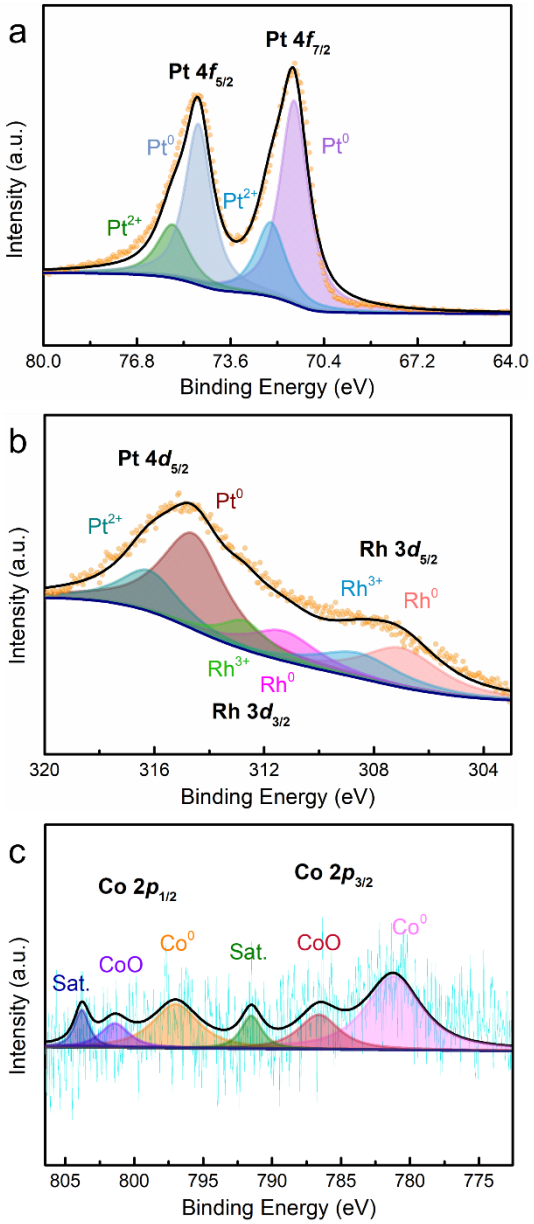

Figure S16. High-resolution PtCoRh/C XPS spectra of Pt 4f (a), Rh 3d (b) and Co 2p (c). Pt 4f displays two pairs of peaks, the stronger pair is attributed to $4f_{5/2}$ and $4f_{7/2}$ of metallic Pt (0) species, and the weaker pair is assigned to Pt (2+) species. In the Rh 3d XPS, the peak of Rh $3d_{3/2}$ is partially overlapped by Pt $4d_{5/2}$, and two types of Rh species in the metallic Rh (0) and oxidation Rh (3+) can be obtained. However, due to the low content, the XPS signal of Co is weak.

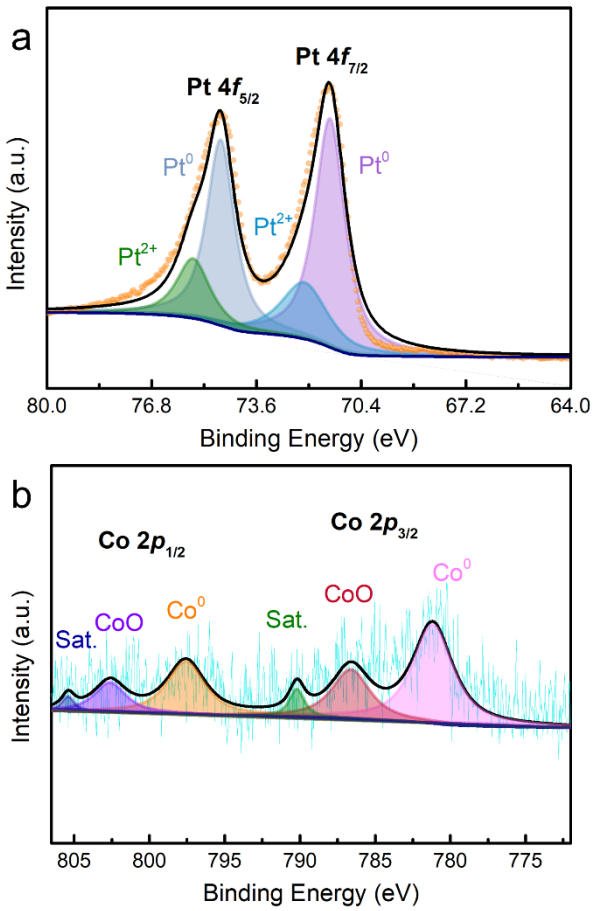

Figure S17. High-resolution PtCo/C XPS spectra of Pt 4f (a) and Co 2p (b).

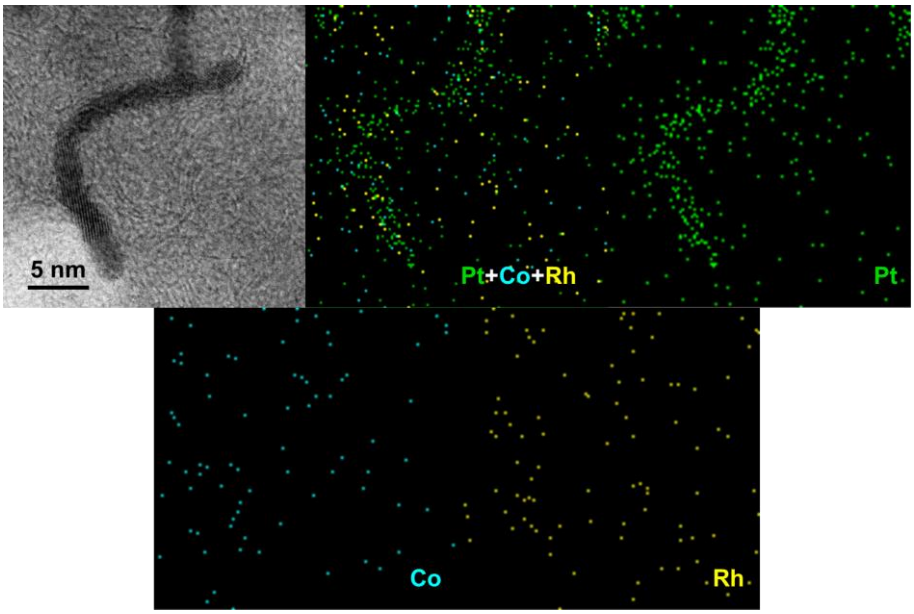

Figure S18. HR-STEM image and corresponding EDS elemental mapping of Pt, Co, and Rh of PtCoRh/C after stability test.

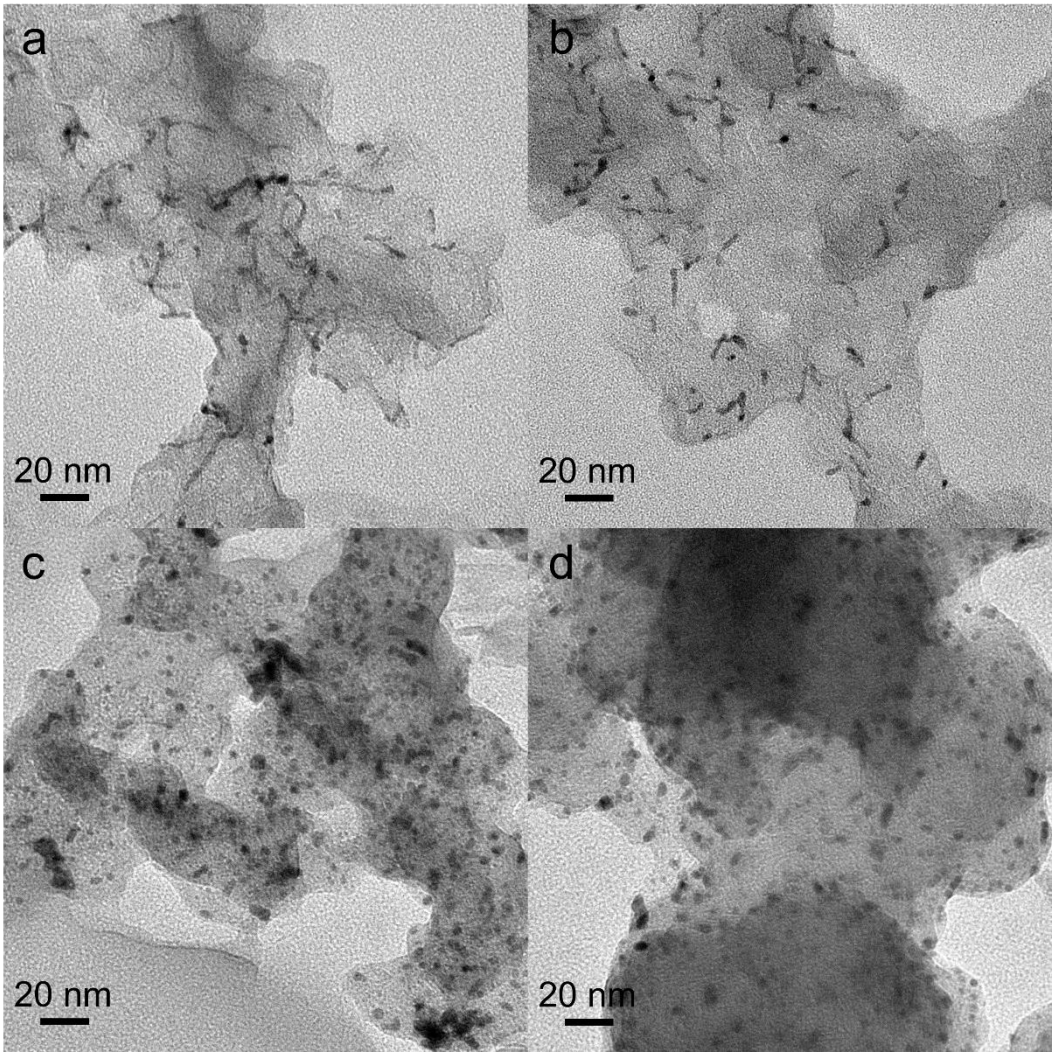

Figure S19. TEM images after stability test: (a, b) PtCoRh/C; (c, d) commercial Pt/C.

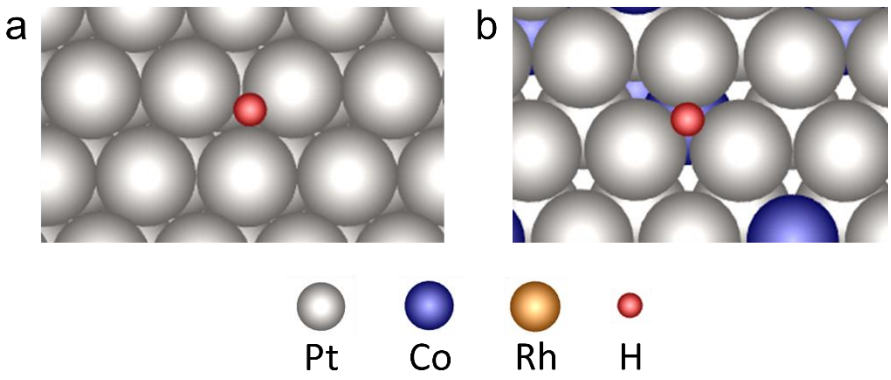

Figure S20. Models of H adsorption on (111) surface of Pt (a) and PtCo (b).

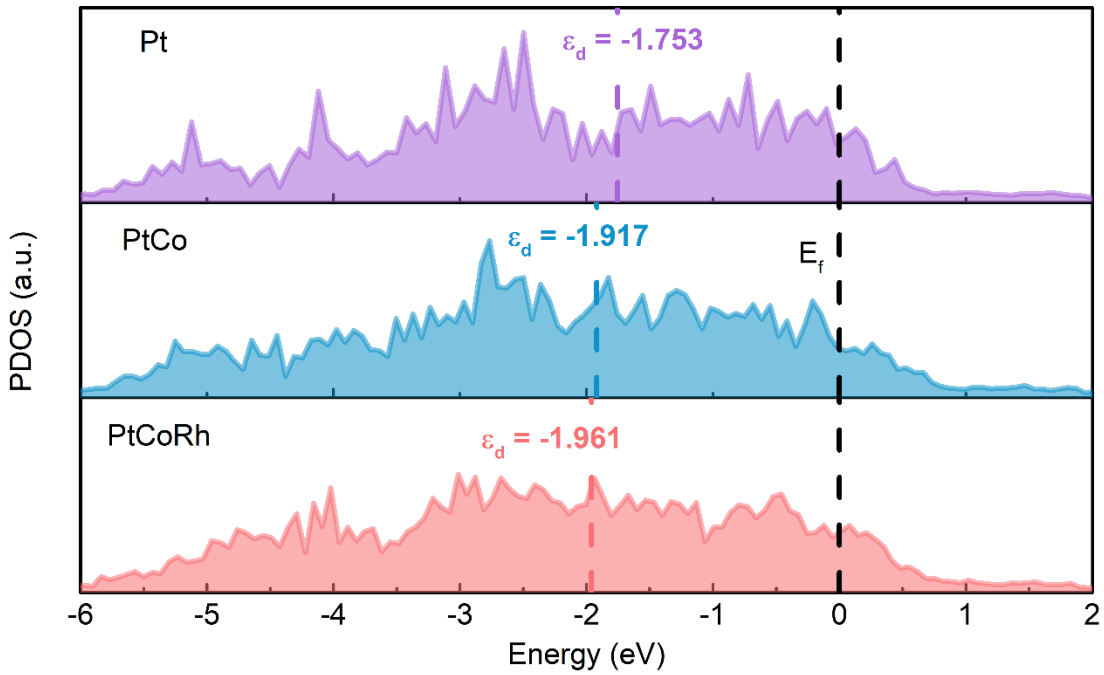

Figure S21. PDOS plots of Pt, PtCo and PtCoRh. The vertical black dash line represents the Fermi level (E_f). ε_d represents d-band center.

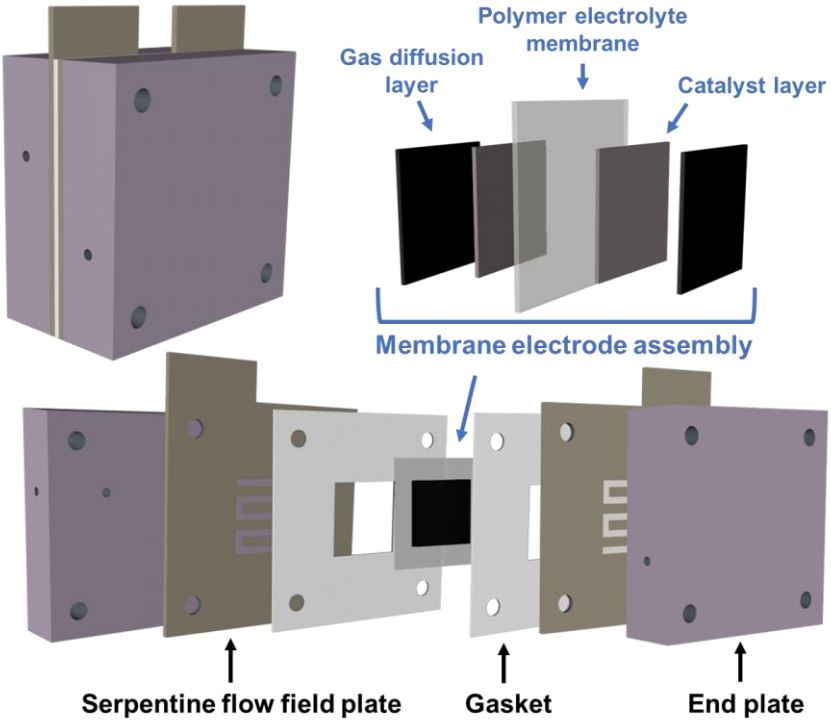

Figure S22. Scheme of the components of a PEMWE.

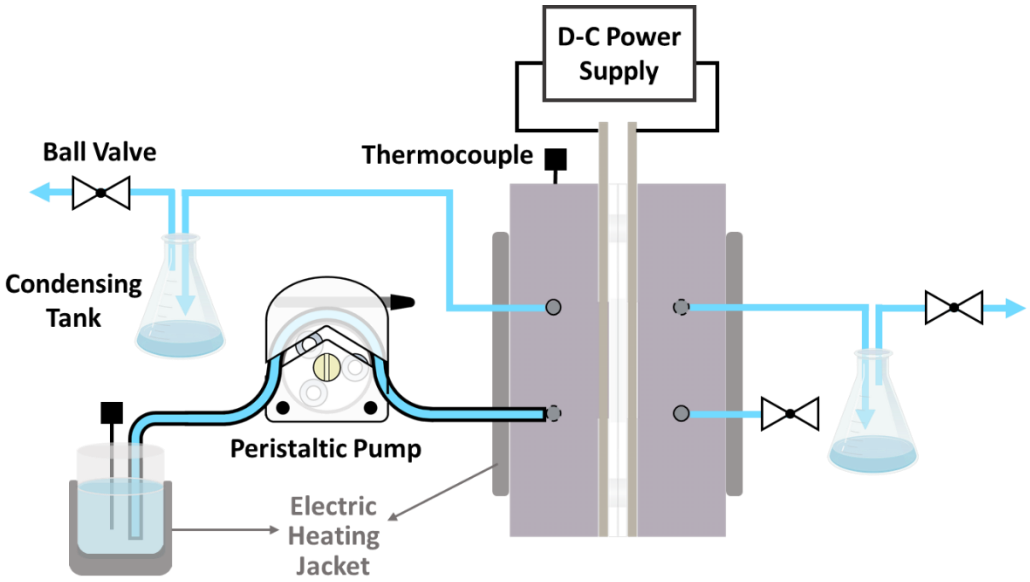

Figure S23. Configuration of house-made PEMWE test station.

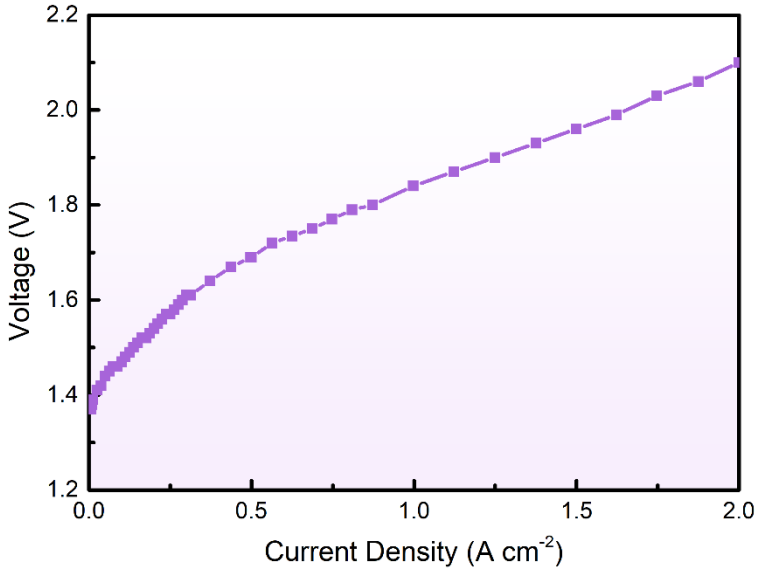

Figure S24. *V-I* curve of a PEMWE obtained at 80 °C and atmospheric pressure fabricated by 0.1 mg_{Pt} cm^{-2} of PtCoRh/C as cathode without iR correction.

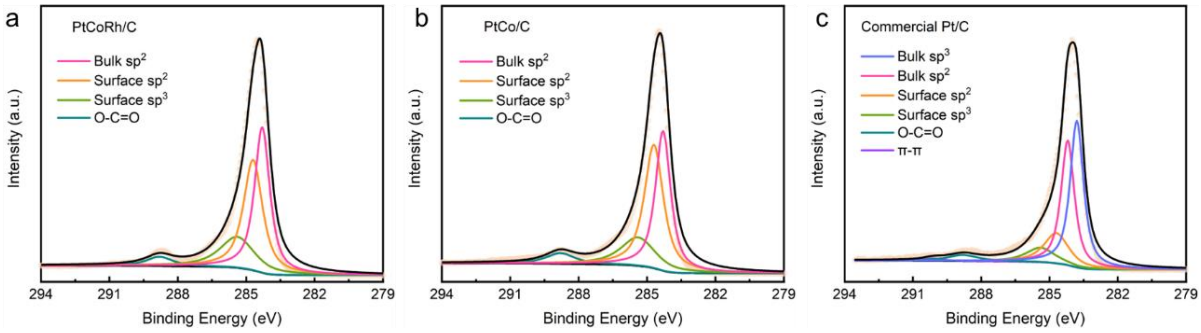

Figure S25. High-resolution C 1s spectra of (a) PtCoRh/C, (b) PtCo/C, and (c) commercial Pt/C, respectively.

Table S1. TGA results of as-obtained electrocatalysts

Sample	Metal loading obtained from TGA
PtCoRh/C	17.0 wt%
PtCoRh/C-2	19.3 wt%
PtCoRh/C-3	21.0 wt%
PtCo/C	16.7 wt%

Table S2. ICP-OES results of as-obtained electrocatalysts

Sample	Elemental atomic ratio obtained from ICP-OES		
	Pt	**Co**	**Rh**
PtCoRh/C	81.5%	16.1%	2.4%
PtCoRh/C-2	79.2%	13.5%	7.3%
PtCoRh/C-3	67.6%	13.7%	18.6%
PtCo/C	85.4%	14.6%	—

Table S3. Acidic HER performance of noble metal based electrocatalysts

Catalyst	Catalyst Loading	Electrolyte	Overpotential (mV)	Current Density (mA cm^{-2})	Reference
PtCoRh/C-1	8 μg_{Pt} cm^{-2}	0.5 M H_2SO_4	6.1	10	This Work
IrCoNi-PHNCs	10 μg_{Ir} cm^{-2}	0.1 M $HClO_4$	33	10	[19]
IrCo-PHNCs	10 μg_{Ir} cm^{-2}	0.1 M $HClO_4$	21	10	
Rh-MoS_2	16 μg_{Rh} cm^{-2}	0.5 M H_2SO_4	47	10	[20]
PtCoFe@CN	13 μg_{Pt} cm^{-2}	0.5 M H_2SO_4	45	10	[21]
PtNC/S-C	2.55 μg_{Pt} cm^{-2}	0.5 M H_2SO_4	11	10	[22]
hollow Pt/NiO/RuO_2/C	14 μg_{PGM} cm^{-2}	0.1 M $HClO_4$	29.6	10	[23]
PtRu@RFCS-6h-0.2%	354 μg cm^{-2} (18 μg_{PGM} cm^{-2})	0.5 M H_2SO_4	19.7	10	[24]
Pt-GT-1	1.4 μg_{Pt} cm^{-2} (~280 μg cm^{-2})	0.5 M H_2SO_4	18	10	[25]
Pt-SAs/WS_2	10.12μg cm^{-2}	0.5 M H_2SO_4	32	10	[26]
Pt SASs/AG	7.07 mg cm^{-2} (31 μg_{Pt} cm^{-2})	0.5 M H_2SO_4	12	10	[27]
Pt_1/NMC	10 μg_{Pt} cm^{-2}	0.5 M H_2SO_4	29	10	[28]
			55	100	
Pt/np-$Co_{0.85}Se$	~2.04 mg cm^{-2} (~21 μg_{Pt} cm^{-2})	0.5 M H_2SO_4	58	10	[29]
Pt_1/hNCNC-2.92	98 μg cm^{-2} (~2.9 μg_{Pt} cm^{-2})	0.5 M H_2SO_4	15	10	[30]
PtCo@PtSn	42.1 μg_{Pt} cm^{-2}	0.5 M H_2SO_4	21	10	[31]
Pt@Co SAs-ZIF-NC	14 μg_{Pt} cm^{-2}	0.5 M H_2SO_4	27	10	[32]
Pt_1/Co_1NC	0.611 mg cm^{-2}	0.5 M H_2SO_4	4.15	10	[33]
Pt-MoO_{3-x} NFs | MoS_2	30 μg_{Pt} cm^{-2}	0.5 M H_2SO_4	69	10	[34]
S-RhNi/C	50.95 μg_{metal} cm^{-2}	0.5 M H_2SO_4	41.78	60	[35]
AL-Pt/Pd_3Pb	40.8 μg_{Pt+Pd} cm^{-2} (1.6 μg_{Pt} cm^{-2})	0.5 M H_2SO_4	13.8	10	[36]
$Pd_{86}Pt_{14}$ NWs	84.93 μg_{Pt+Pd} cm^{-2} (19.52 μg_{Pt} cm^{-2})	0.5 M H_2SO_4	0.8	10	[37]
Pt-AC/DG-500	~0.1 mg cm^{-2} (~3.5 μg_{Pt} cm^{-2})	0.1 M $HClO_4$	21	10	[38]
RhCo-ANAs	2 mg cm^{-2}	0.5 M H_2SO_4	12.4	10	[39]

References

1. H. Li, Y. Pan, D. Zhang, Y. Han, Z. Wang, Y. Qin, S. Lin, X. Wu, H. Zhao, J. Lai, B. Huang and L. Wang, *J. Mater. Chem. A*, 2020, **8**, 2323-2330.
2. L. Bu, S. Guo, X. Zhang, X. Shen, D. Su, G. Lu, X. Zhu, J. Yao, J. Guo and X. Huang, *Nat. Commun.*, 2016, **7**, 11850.
3. K. Jiang, D. Zhao, S. Guo, X. Zhang, X. Zhu, J. Guo, G. Lu and X. Huang, *Sci. Adv.*, 2017, **3**, e1601705.
4. C. Qiu, H. Chen, H. Liu, Z. Zhai, J. Qin, Y. Lv, Z. Gao and Y. Song, *Int. J. Hydrogen Energy*, 2018, **43**, 21908-21917.
5. S. Takabayashi, K. Okamoto, K. Shimada, K. Motomitsu, H. Motoyama, T. Nakatani, H. Sakaue, H. Suzuki and T. Takahagi, *Jpn. J. Appl. Phys.*, 2008, **47**, 3376–3379.
6. S. Takabayashi, K. Motomitsu, T. Takahagi, A. Terayama, K. Okamoto and T. Nakatani, *J. Appl. Phys.*, 2007, **101**, 103542.
7. Y. Lv, H. Liu, J. Li, J. Chen and Y. Song, *J. Electroanal. Chem.*, 2020, **870**, 114172.
8. Y. Lv, H. Liu, J. Qin, R. Gao, Y. Zhang, Y. Xie, J. Li and Y. Song, *Prog. Nat. Sci-Mater*, 2020, **30**, 832-838.
9. G. Kresse and J. Furthmüller, *Phys. Rev. B*, 1996, **54**, 11169-11186.
10. G. Kresse and J. Hafner, *Phys. Rev. B*, 1993, **47**, 558-561.
11. P. E. Blöchl, *Phys. Rev. B*, 1994, **50**, 17953-17979.
12. J. P. Perdew, K. Burke and M. Ernzerhof, *Phys. Rev. Lett.*, 1996, **77**, 3865-3868.
13. Y. Zhang and W. Yang, *Phys. Rev. Lett.*, 1998, **80**, 890-890.
14. B. Hammer, L. B. Hansen and J. K. Nørskov, *Phys. Rev. B*, 1999, **59**, 7413-7421.
15. H. J. Monkhorst and J. D. Pack, *Phys. Rev. B*, 1976, **13**, 5188-5192.
16. J. K. Nørskov, T. Bligaard, A. Logadottir, J. R. Kitchin, J. G. Chen, S. Pandelov and U. Stimming, *J. Electrochem. Soc.*, 2005, **152**, J23-J26.
17. D. Li, M. H. Nielsen, J. R. Lee, C. Frandsen, J. F. Banfield and J. J. De Yoreo, *Science*, 2012, **336**, 1014-1018.
18. C. Wang, Y. Hou, J. Kim and S. Sun, *Angew. Chem. Int. Ed.*, 2007, **46**, 6333-6335.
19. J. Feng, F. Lv, W. Zhang, P. Li, K. Wang, C. Yang, B. Wang, Y. Yang, J. Zhou, F. Lin, G. C. Wang and S. Guo, *Adv. Mater.*, 2017, **29**, 1703798.
20. Y. Cheng, S. Lu, F. Liao, L. Liu, Y. Li and M. Shao, *Adv. Funct. Mater.*, 2017, **27**, 1700359.
21. J. Chen, Y. Yang, J. Su, P. Jiang, G. Xia and Q. Chen, *ACS Appl. Mater. Interfaces*, 2017, **9**, 3596-3601.
22. Q. Q. Yan, D. X. Wu, S. Q. Chu, Z. Q. Chen, Y. Lin, M. X. Chen, J. Zhang, X. J. Wu and H. W. Liang, *Nat. Commun.*, 2019, **10**, 4977.
23. A. Oh, H. Y. Kim, H. Baik, B. Kim, N. K. Chaudhari, S. H. Joo and K. Lee, *Adv. Mater.*, 2019, **31**, 1805546.
24. K. Li, Y. Li, Y. Wang, J. Ge, C. Liu and W. Xing, *Energy Environ. Sci.*, 2018, **11**, 1232-1239.
25. J. N. Tiwari, S. Sultan, C. W. Myung, T. Yoon, N. Li, M. Ha, A. M. Harzandi, H. J. Park, D. Y. Kim, S. S. Chandrasekaran, W. G. Lee, V. Vij, H. Kang, T. J. Shin, H. S. Shin, G. Lee, Z. Lee and K. S. Kim, *Nat. Energy*, 2018, **3**, 773-782.
26. Y. Shi, Z. R. Ma, Y. Y. Xiao, Y. C. Yin, W. M. Huang, Z. C. Huang, Y. Z. Zheng, F. Y. Mu, R. Huang, G. Y. Shi, Y. Y. Sun, X. H. Xia and W. Chen, *Nat. Commun.*, 2021, **12**, 3021.
27. S. Ye, F. Luo, Q. Zhang, P. Zhang, T. Xu, Q. Wang, D. He, L. Guo, Y. Zhang, C. He, X. Ouyang, M. Gu, J. Liu and X. Sun, *Energy Environ. Sci.*, 2019, **12**, 1000-1007.
28. H. Wei, H. Wu, K. Huang, B. Ge, J. Ma, J. Lang, D. Zu, M. Lei, Y. Yao, W. Guo and H. Wu, *Chem. Sci.*, 2019, **10**, 2830-2836.
29. K. Jiang, B. Liu, M. Luo, S. Ning, M. Peng, Y. Zhao, Y. R. Lu, T. S. Chan, F. M. F. de Groot and Y. Tan, *Nat. Commun.*, 2019, **10**, 1743.
30. Z. Zhang, Y. Chen, L. Zhou, C. Chen, Z. Han, B. Zhang, Q. Wu, L. Yang, L. Du, Y. Bu, P. Wang, X. Wang, H. Yang and Z. Hu, *Nat. Commun.*, 2019, **10**, 1657.
31. J. Chen, G. Qian, H. Zhang, S. Feng, Y. Mo, L. Luo and S. Yin, *Adv. Funct. Mater.*, 2021, **32**, 2107597.
32. L. Liang, H. Jin, H. Zhou, B. Liu, C. Hu, D. Chen, Z. Wang, Z. Hu, Y. Zhao, H.-W. Li, D. He and S. Mu, *Nano Energy*, 2021, **88**, 106221.

33. Y. Chen, R. Ding, J. Li and J. Liu, *Appl. Catal. B : Environ.*, 2022, **301**, 120830.
34. D. Lee, Y. Kim, H. W. Kim, M. Choi, N. Park, H. Chang, Y. Kwon, J. H. Park and H. J. Kim, *J. Catal.*, 2020, **381**, 1-13.
35. J. Lu, Z. Tang, L. Luo, S. Yin, P. Kang Shen and P. Tsiakaras, *Appl. Catal. B : Environ.*, 2019, **255**, 117737.
36. Y. Yao, X. K. Gu, D. He, Z. Li, W. Liu, Q. Xu, T. Yao, Y. Lin, H. J. Wang, C. Zhao, X. Wang, P. Yin, H. Li, X. Hong, S. Wei, W. X. Li, Y. Li and Y. Wu, *J. Am. Chem. Soc.*, 2019, **141**, 19964-19968.
37. H. Lv, X. Chen, D. Xu, Y. Hu, H. Zheng, S. L. Suib and B. Liu, *Appl. Catal. B : Environ.*, 2018, **238**, 525-532.
38. Q. Cheng, C. Hu, G. Wang, Z. Zou, H. Yang and L. Dai, *J. Am. Chem. Soc.*, 2020, **142**, 5594-5601.
39. Y. Zhao, J. Bai, X.-R. Wu, P. Chen, P.-J. Jin, H.-C. Yao and Y. Chen, *J. Mater. Chem. A*, 2019, **7**, 16437-16446.